HHS Public Access

Author manuscript

Exp Neurol. Author manuscript; available in PMC 2019 May 01.

Published in final edited form as:

Exp Neurol. 2018 May ; 303: 108–119. doi:10.1016/j.expneurol.2018.02.007.

Cell-type specific expression of constitutively-active Rheb promotes regeneration of bulbospinal respiratory axons following cervical SCI

Mark W. Urban[a], **Biswarup Ghosh**[a], **Laura R. Strojny**[a], **Cole G. Block**[a], **Sara M. Blazejewski**[a], **Megan C. Wright**[b], **George M. Smith**[c], and **Angelo C. Lepore**[a,*]

[a]Department of Neuroscience, Vickie and Jack Farber Institute for Neuroscience, Sidney Kimmel Medical College at Thomas Jefferson University, 233 South 10th Street, BLSB 245, Philadelphia, PA, 19107, United States

[b]Department of Biology, Arcadia University, 450 S. Easton Rd., 220 Boyer Hall, Glenside, PA, 19038, United States

[c]Department of Neuroscience, Shriners Hospitals for Pediatric Research Center, Temple University School of Medicine, 3500 North Broad Street, Philadelphia, PA, 19140-5104, United States

Abstract

Damage to respiratory neural circuitry and consequent loss of diaphragm function is a major cause of morbidity and mortality in individuals suffering from traumatic cervical spinal cord injury (SCI). Repair of CNS axons after SCI remains a therapeutic challenge, despite current efforts. SCI disrupts inspiratory signals originating in the rostral ventral respiratory group (rVRG) of the medulla from their phrenic motor neuron (PhMN) targets, resulting in loss of diaphragm function. Using a rat model of cervical hemisection SCI, we aimed to restore rVRG-PhMN-diaphragm circuitry by stimulating regeneration of injured rVRG axons via targeted induction of Rheb (Ras homolog enriched in brain), a signaling molecule that regulates neuronal-intrinsic axon growth potential. Following C2 hemisection, we performed intra-rVRG injection of an adeno-associated virus serotype-2 (AAV2) vector that drives expression of a constitutively-active form of Rheb (cRheb). rVRG neuron-specific cRheb expression robustly increased mTOR pathway activity within the transduced rVRG neuron population ipsilateral to the hemisection, as assessed by levels of phosphorylated ribosomal S6 kinase. By co-injecting our novel AAV2-mCherry/WGA anterograde/trans-synaptic axonal tracer into rVRG, we found that cRheb expression promoted regeneration of injured rVRG axons into the lesion site, while we observed no rVRG axon regrowth with AAV2-GFP control. AAV2-cRheb also significantly reduced rVRG axonal dieback

[*]Corresponding author: Angelo C. Lepore, Ph.D., Department of Neuroscience, Vickie and Jack Farber Institute for Neuroscience, Sidney Kimmel Medical College at Thomas Jefferson University, 233 South 10th Street, BLSB 245, Philadelphia, PA, 19107, United States, Phone: 610-564-3375, angelo.lepore@jefferson.edu.

Conflicts of interest: none.

within the intact spinal cord rostral to the lesion. However, cRheb expression did not promote any recovery of ipsilateral hemi-diaphragm function, as assessed by inspiratory electromyography (EMG) burst amplitudes. This lack of functional recovery was likely because regrowing rVRG fibers did not extend back into the caudal spinal cord to synaptically reinnervate PhMNs that we retrogradely-labeled with cholera toxin B from the ipsilateral hemi-diaphragm. Our findings demonstrate that enhancing neuronal-intrinsic axon growth capacity can promote regeneration of injured bulbospinal respiratory axons after SCI, but this strategy may need to be combined with other manipulations to achieve reconnection of damaged neural circuitry and ultimately recovery of diaphragm function.

Keywords

cervical spinal cord injury; diaphragm; respiratory; breathing; axon; regeneration; regrowth; Rheb; mTOR; AAV2

Introduction

Regeneration of central nervous system (CNS) axons after spinal cord injury (SCI) remains a clinical challenge, and while studies have shown that CNS regeneration is possible, reconnection to original secondary neuronal targets remains, as a whole, elusive (Alilain et al., 2011; Cafferty et al., 2008; Mantilla, 2017; Park et al., 2010; Vinit et al., 2006). The lack of a robust axonal regrowth response plays a significant role in persistent functional deficits following SCI. Furthermore, targeted regeneration within the CNS is important for repair of motor, sensory and other functions post-SCI as incorrect targeting of growing axons could not only result in failure to restore damaged circuitry, but also in unwanted side effects (Harel and Strittmatter, 2006). A number of factors, both neuronal-intrinsic and -extrinsic, impede axon regeneration following CNS injury (Busch and Silver, 2007; Cregg et al., 2014; Dell'Anno and Strittmatter, 2017; Fitch and Silver, 2008; Gervasi et al., 2008; Yiu and He, 2006). Low endogenous axonal growth capacity represents a critical impediment inhibiting regeneration of most adult CNS neurons (Lu et al., 2014; Ribas and Costa, 2017). In particular, the mammalian target of rapamycin (mTOR) pathway, a master regulator of cellular growth, protein synthesis and axon development, remains in an inactive state following CNS damage (Liu et al., 2010; Park et al., 2008). Previous studies suggest that altering the expression of molecules within this signaling axis such as genetic knockout of phosphatase and tensin homolog (PTEN) and overexpression of ras homolog enriched in brain (Rheb) can lead to robust regeneration of certain neuronal populations (Danilov and Steward, 2015; Gutilla and Steward, 2016; Liu et al., 2010; Ohtake et al., 2015; Park et al., 2008; Zukor et al., 2013). Rheb directly binds to the mTOR complex, and the active GTP-bound form of Rheb is required for mTOR activation (Duran and Hall, 2012; Long et al., 2005). Additionally, inhibition of this Rheb-mTOR pathway is mediated by the tumor sclerosis complex proteins 1/2 (TSC1/2) (Zhang et al., 2003), which function as GTPase-activating proteins (GAPs) to convert the GTP-bound Rheb to an inactivated GDP-bound form. Altering the expression pattern and function of these molecules within the mTOR pathway has the potential to induce regrowth of damaged axons (including back to their original targets), ultimately resulting in functional restoration.

SCI is a devastating disorder characterized by damage to ascending, descending and intra-segmental neuronal connections. Individuals suffering from cervical injuries often experience difficulty breathing (as well as other pulmonary deficits) due to loss of medullary input to spinal cord, ultimately resulting in partial-to-complete paralysis of diaphragm, a major inspiratory muscle (Vinit and Kastner, 2009). Consequently, many cervical SCI patients must be mechanically ventilated, which leads to enhanced morbidity as well as increased mortality as a result of complications such as respiratory infection (University of Alabama, 2016).

Diaphragm activation is directly controlled by phrenic motor neurons (PhMNs) located within the ventral horn at C3 to C5 levels of the spinal cord (Dobbins and Feldman, 1994). PhMNs receive rhythmic descending glutamatergic input from bulbospinal axons originating in the rostral ventral respiratory group (rVRG) of the medulla; this rVRG-PhMN circuitry is primarily monosynaptic (Lipski et al., 1994). Though some rVRG axons do cross to the contralateral PhMN pool, these connections appear to be latent in intact conditions (Ghali, 2017). Cervical SCI disrupts rVRG axonal input to their PhMN targets and consequently produces loss of hemi-diaphragm function(Vinit et al., 2006). Restoration of this circuitry remains a critical, though elusive, therapeutic goal.

Adeno-associated viruses (AAVs) are powerful tools for altering the expression of specific genes in a defined neuronal population within the CNS. In the current study, we tested the effects on rVRG regeneration of expressing a constitutively-active form of Rheb (AAV2-cRheb) selectively in axotomized rVRG neurons following C2 hemisection SCI. As Rheb is highly unstable in the GDP-bound state, we generated an AAV2 construct to express a mutated GTP-bound active form of the Rheb protein. With this strategy, we aimed to enhance the neuronal-intrinsic capacity of rVRG neurons to repair damaged respiratory circuitry and restore diaphragm function after cervical SCI.

Materials and methods

Animals

Female Sprague-Dawley rats weighing 250-300 grams were purchased from Taconic Farms. All animals were housed three animals per cage in temperature, humidity, and light controlled environments with *ad libitum* access to food and water. Experimental procedures were approved by the Thomas Jefferson University IACUC and conducted in compliance with ARRIVE (*Animal Research: Reporting of In Vivo Experiments*) guidelines.

C2 hemisection SCI

Rats were deeply anesthetized with an intraperitoneal injection of a cocktail of ketamine HCl (95.0mg/kg) (Vedco, Saint Joseph, Missouri), xylazine (10.0mg/kg) (Lloyd Laboratories, Quezon City, Metro Manila, Philippines) and acepromazine (0.075mg/kg) (Phoenix Pharm Inc, Burlingame, California). Once the rats were completely anesthetized, assessed via loss of toe pinch reflex and orbital reflex, the dorsal surface of the skin was shaved and disinfected with a 70% ethanol solution and topical iodine (Dynarex, Orangeburg, New York). Using a sterile #11 surgical blade (Electron Microscopy Sciences,

Hatfield, Pennsylvania). A one-inch midline incision was made on the dorsal surface of skin and muscle starting from the caudal portion of the occipital bone. Retractors were then used to expose the dorsal surface of the C2 and C3 vertebrae. Using rongeurs (Fine Science Tools, Foster City, California), remaining tissue was removed from the vertebrae and a laminectomy was performed to expose the spinal cord. The C2 and C3 dorsal roots were located, and a hemisection was performed at a location just caudal to the C2 root with a dissecting knife (Fine Science Tools, Foster City, California). To ensure a complete hemisection, a 30-gauge needle (BD Biosciences, San Jose, California) was passed through the injury several times. Following complete hemisection, the dorsal muscle layers were sutured with 4-0 silk sutures (Covidien, Minneapolis, Minnesota), and the skin was stapled closed with surgical staples (Braintree Scientific, Braintree, Massachusetts). The surface of the skin was treated with a topical iodine solution. Immediately following the procedure, rats were treated with 5mL subcutaneous injections of Lactated Ringer's solution (Hospira, San Jose, California), buprenorphine hydrochloride (0.05mg/kg) (Hospira, San Jose, California) and cefazolin (6 mg) (Hospira, San Jose, California). Rats were then placed in a clean cage on a surgical heating pad set to 37°C (Gaymar, Orchard Park, New York) and monitored until fully recovered from anesthesia. At both 12 and 24 hours after surgery, each rat was given an additional dose of buprenorphine hydrochloride (0.05mg/kg) and 5mL of Lactated Ringer's solution and monitored for pain/distress. Rats were subsequently monitored daily for pain, as well as for forepaw and hindpaw autophagy.

rVRG injection

Rats were anesthetized with a mixture of ketamine/xylazine/acepromazine. Previous surgical staples were removed using a reflex clip remover. The skin was shaved and then disinfected with a 70% ethanol solution and topical iodine. Using a sterile #11 surgical blade, a half-inch incision was made on the dorsal surface of the skin at the occipital bone, and surgical scissors (Fine Science Tools, Foster City, California) were used to separate the superficial muscle, exposing the occipital bone and C1 vertebrae. The skin and muscles were separated with a surgical retractor (Fine Science Tools, Foster City, California), and using a surgical blade and rongeurs, the ligament between the occipital bone and the C1 vertebrae was excised followed by removal of the caudal portion of the occipital bone revealing the obex. The animals were then placed on a stereotaxic frame (Kopf Instruments, Tujunga, California). Using the obex as a starting point, the rVRG was located by the following coordinates: 2.0 mm lateral, 1.0 mm rostral, and 2.6 mm ventral. Once properly placed, an UltraMicroPump (World Precision Instruments, Sarasota, Florida) injection system was used to inject 0.3 microliters of total volume using a microsyringe (Hamilton, Reno, Nevada) and a Micro4 Microsyringe Pump Controller (World Precision Instruments, Sarasota, Florida). Immediately following injection, the needle was left in place for 5 minutes before being slowly removed from the medulla. The retractor was removed, the muscles were sutured with 4-0 silk sutures, and the skin was stapled closed and disinfected with topical iodine as described above. Rats were then placed in a clean cage and given post-operative treatment, as described above.

Diaphragm injection

Rats were anesthetized with a mixture of ketamine/xylazine/acepromazine. Animals were placed supine, and a laparotomy was performed starting from the xyphoid process and cutting laterally just below the rib cage to expose the right hemi-diaphragm. Once exposed, Cholera Toxin Subunit B (CTB) Recombinant, Alexa Fluor 647 Conjugate (Life Technologies, Waltham, Massachusetts) was injected into the ventral, medial and dorsal portions of the hemi-diaphragm with 5 μl injected per site, specifically targeting the endplate band. Following injections, the muscles were sutured, and the skin was stapled closed. The surface of the skin was treated with a topical iodine solution. Rats were then treated with Lactated Ringer's solution, buprenorphine, and cefazolin and monitored daily for pain/distress, as described above.

Electromyography (EMG) recordings

Animals were anesthetized with a cocktail of ketamine/xylazine/acepromazine as discussed above. Once deeply anesthetized, a laparotomy was performed to expose the right hemi-diaphragm similar to diaphragm injections. Bipolar electrodes spaced 3 mm apart were placed for recording in three separate sub-regions of the hemi-diaphragm: dorsal, medial, and ventral. Recordings were averaged over a five-minute time frame for each animal, and peak amplitude, burst duration and frequency were taken. Using LabChart 7 software (ADInstruments, Colorado Springs, Colorado), the EMG signal was amplified and filtered through a band-pass filter (50-3000 Hz).

Compound Muscle Action Potential (CMAP) recordings

Rats were anesthetized with isoflurane (Piramal Healthcare, Bethlehem, Pennsylvania) at a concentration of 3.0-3.5% diluted in oxygen. Animals were placed supine and the region just below the rib cage was shaved and cleaned with 70% ethanol. Phrenic nerve conduction studies were performed with stimulation at the neck via near nerve needle electrodes placed along the phrenic nerve. A reference electrode was placed on the shaved surface of the right costal region. The phrenic nerve was stimulated with a single burst at 6mV (amplitude) for a 0.5 millisecond duration. Each animal was stimulated between 10-20 times to ensure reproducibility, and recordings were averaged for analysis. ADI Powerlab8/30stimulator and BioAMPamplifier (ADInstruments, Colorado Springs, CO) were used for both stimulation and recording, and Scope 3.5.6 software (ADInstruments, Colorado Springs, CO) was used for subsequent data analysis. Following recordings, animals were immediately euthanized with a triple-dose of ketamine/xylazine/acepromazine and tissue was collected (as described below).

Spinal cord and brainstem dissection

Animals were euthanized with a mixture of ketamine/xylazine/acepromazine. After the right hemi-diaphragm was excised, a small cut of right atrium was made to exsanguinate the animal. Next, a needle was placed into the left ventricle and a 0.9% saline solution (Fisher Scientific, Pittsburgh, Pennsylvania) was perfused through to clear the animal. Once the animal was cleared of blood, a 4% paraformaldehyde solution (Electron Microscopy Sciences, Hatfield, Pennsylvania) was perfused to fix the tissue. Following fixation, the

spinal cord and brain were excised with rongeurs (Fine Science Tools, Foster City, California) and kept in a 4% paraformaldehyde solution overnight at 4°C. The following morning, samples were washed with a 0.1 M Phosphate Buffer solution (Sodium Phosphate Dibasic Heptahydrate (Sigma-Aldrich, St. Louis, Missouri) and Sodium Monobasic Monohydrate (Sigma-Aldrich, St. Louis, Missouri)) for 24 hours. Samples were then placed in 30% sucrose (Sigma-Aldrich, St. Louis, Missouri) for approximately 72 hours, samples were then submerged in an embedding mold (Polysciences Inc, Warrington, Pennsylvania) and covered with tissue freezing medium (General Data, Cincinnati, Ohio). Samples were then flash frozen in 2-methylbutane (Fisher Scientific, Pittsburgh, Pennsylvania) chilled in dry ice. Tissue sections were stored at −80°C until sectioned on a cryostat (Thermo Scientific, Philadelphia, Pennsylvania). Brainstem (transverse) and spinal cord (sagittal) sections were cut at 30 μm, placed on glass slides (Fisher Scientific, Pittsburgh, Pennsylvania), dried overnight, and stored at −20°C for histological analysis.

Immunohistochemistry

Tissue sections were retrieved from −20°C freezer and dried for 1 hour at room temperature, followed by antigen retrieval using R&D Systems Protocol (R&D Systems, Minneapolis, Minnesota). Immediately after antigen retrieval, slide edges were dried and a hydrophobic pen was used to surround the tissue sections (Newcomer Supply, Middleton, Wisconsin). A blocking/permeabilization step was conducted for 1 hour at room temperature with a solution of 5% Normal Horse Serum (Vector Laboratories, Burlingame, California), 0.2% Triton X-100 (Amresco, Solon, Ohio), diluted in PBS (primary and secondary antibodies were diluted in this solution as well). Tissue sections were then treated with primary antibody overnight at 4°C with the following antibodies: Neuronal marker anti-NeuN at 1:200 (EMD-Millipore, Temecula, California), astrocyte marker anti-GFAP at 1:400 (Dako, Carpinteria, California), oligodendrocyte lineage marker anti-Olig-2 at 1:200 (EMD-Millipore, Temecula, California), anti-HA tag at 1:200 (Sigma-Aldrich, St. Louis, Missouri), anti-Phospho-S6 Ribosomal Protein (Ser235/236) at 1:50 (Cell Signaling Technology, Danvers, Massachusetts), anti-wheat germ agglutinin (WGA) at 1:50 (Vector Laboratories, Burlingame, California). On the following morning, samples were washed 3× in PBS, and secondary antibody solutions were added for 1 hour at room temperature: donkey anti-rabbit IgG H&L (Alexa Fluor 647) at 1:200 (Abcam, Cambridge, Massachusetts), donkey anti-mouse IgG H&L (Alexa Fluor 488) at 1:200 (Abcam, Cambridge, Massachusetts), Rhodamine (TRITC) AffiniPure donkey anti-goat IgG (H+L) at 1:200 (Jackson ImmunoResearch, West Grove, Pennsylvania). Following secondary antibody treatment, samples were washed 3× in PBS. 2–3 drops of FluorSave reagent (Calbiochem, San Diego, California) was added to tissue sections, and coverslips (Fisher Scientific, Pittsburgh, Pennsylvania) were added. Slides were left to dry for 30 minutes at room temperature in the dark and then kept at 4°C.

Spinal cord histology

Tissue sections were retrieved from the −20°C freezer and dried at room temperature for 2 hours. Slides were then placed in 3-minute baths of xylene, 100% ethanol, 95% ethanol, 70% ethanol and dH_2O. Slides were next placed in an ErioChrome solution (0.16% Eriochrome Cyanine, 0.4% Sulfuric Acid, 0.4% Ferric Chloride in dH_2O) for 14 minutes,

washed with tap water, placed in a developing solution (0.3% ammonium hydroxide in dH_2O) for 5 minutes, washed with dH_2O, and then placed into a cresyl violet solution (0.4% cresyl violet, 6% 1M sodium acetate, 34% 1M acetic acid) for 18 minutes. Finally, slides were placed in baths of dH_2O, 70% ethanol, 95% ethanol, 100% ethanol and xylene. Slides were then mounted with poly-mount xylene (Polysciences, Warrington, Pennsylvania) and cover slips were added. Slides were then kept at room temperature for analysis.

pS6K70 immunofluorescence quantification

To determine activation of pS6K70, brainstem sections were immunostained with anti-Phospho-S6 Ribosomal Protein (Ser235/236) at 1:50 (Cell Signaling Technology, Danvers, Massachusetts), followed by donkey anti-mouse IgG H&L (Alexa Fluor 488) at 1:200 (Abcam, Cambridge, Massachusetts). Individual rVRG neurons were traced manually in ImageJ/Fiji software, using images captured via 20× objective on a Zeiss Axio M2 Imager (Carl Zeiss Inc., Thornwood, New York). Mean intensity per cell was measured using ImageJ/Fiji software. Average background intensity values were subtracted from individual neurons to obtain each intensity value. Average neuronal intensities were recorded and resulting values were quantified using three images per animal; 4 and 5 animals used for AAV2-GFP and AAV2-cRheb, respectively.

rVRG axon regeneration quantification

30μm sagittal sections of spinal cord tissue were imaged with a Zeiss Axio M2 Imager (Carl Zeiss Inc., Thomwood, New York) to detect mCherry anterograde tracer expression. The high-magnification images were then optically “stitched” using Metamorph software to generate mosaics of the cervical spinal cord. The stitched images were rostral-caudally binned in 100μm segments using the rostral border of the injury and rostral intact spinal cord as the starting point. All mCherry-labeled axons were counted; axons that traversed through more than one bin were counted in all bins that they traversed.

Diaphragm dissection

Animals were euthanized with a mixture of ketamine/xylazine/acepromazine. Animals were placed supine; two incisions were made into the skin and underlying muscle starting from the xyphoid process and extending laterally along the rib cage to expose the right hemi-diaphragm. The right hemi-diaphragm was excised using spring scissors (Fine Science Tools, Foster City, California), stretched flat and pinned down on silicon-coated 10 cm dishes, and washed with PBS (Gibco, Pittsburgh, Pennsylvania). Next, a 20-minute fixation in 4% paraformaldehyde (Electron Microscopy Sciences, Hatfield, Pennsylvania) was performed, followed by several washes in PBS. After washing, superficial fascia was carefully removed from the surface of the diaphragm with Dumont #5 Forceps (Fine Science Tools, Foster City, California). Diaphragms were then stained for NMJ markers (described below).

Diaphragm whole-mount histology

Fresh hemi-diaphragm muscle was dissected from each animal for whole-mount immunohistochemistry, as described previously (Wright and Son, 2007). Diaphragms were

rinsed 3× in PBS and then incubated in 0.1 M glycine for 30 minutes. Following glycine incubation, α-bungarotoxin conjugated to Alexa Fluor 555 at 1:200 (Life Technologies, Waltham, Massachusetts) was used to label post-synaptic nicotinic acetylcholine receptors for 15 minutes and then washed 3× in PBS. Ice-cold methanol was then added to the diaphragms for 5 minutes and then washed 3× in PBS. Diaphragms were then blocked for 1 hour at room temperature in a solution of 2% bovine serum albumin and 0.2% Triton X-100 diluted in PBS (this solution was used for both primary and secondary antibody dilutions). Primary antibodies were added overnight at 4°C: pre-synaptic vesicle marker anti-SV2 at 1:10 (Developmental Studies Hybridoma Bank, Iowa City, Iowa), neurofilament marker anti-SMI-312 at 1:1000 (Covance, Greenfield, Indiana). On the following morning, the diaphragms were washed 3× in blocking solution, and secondary antibody solution was then added for 1 hour at room temperature: FITC anti-mouse IgG secondary (Jackson ImmunoResearch Laboratories, West Grove, PA; 1:100), followed by washing 3× in PBS. Diaphragms were mounted with Vectashield mounting medium (Vector Laboratories, Burlingame, California), coverslips were added, and slides were stored at −20°C.

Neuromuscular junction (NMJ) analysis

Labeled muscles were analyzed for total numbers of NMJs and intact, partially-denervated or completely denervated NMJs. Whole-mounted diaphragms were imaged on a FluoView FV1000 confocal microscope (Olympus, Center Valley, Pennsylvania). We conducted NMJ analysis on only ipsilateral hemi-diaphragm because our previous published work showed no denervation or sprouting in contralateral hemi-diaphragm after cervical injury (Nicaise et al., 2012a; Nicaise et al., 2012b).

Statistics

Data was expressed as means ± standard error of the mean (SEM). Statistical significance was assessed by analysis of variance (one-way ANOVA) and multiple comparisons *post hoc* test. Graphpad Prism 6 (Graphpad Software Inc.) was used to calculate all analyses and $p < 0.05$ was considered significant.

Results

C2 hemisection completely disrupted ipsilateral hemi-spinal cord

To assess repair of rVRG-PhMN-diaphragm respiratory circuitry, we first ensured complete ablation of descending ipsilateral input to the PhMN pool. rVRG-PhMN respiratory drive is predominantly an ipsilateral pathway under intact conditions, making C2 hemisection an effective model for disrupting one hemi-diaphragm while maintaining contralateral hemi-diaphragm function (Fig 1A). Contralateral sparing ensures animal survival post-hemisection and allows for investigation of regrowth of injured ipsilateral rVRG axons. We performed hemisection at the caudal end of the C2 dorsal root to completely spare the PhMN population, which resides in C3-C5 ventral horn (Fig 1B). Additionally, although rVRG axons run primarily in the ventrolateral white matter of the spinal cord, there is a small population of fibers that also runs medially within the ventral funiculus. Therefore, to unambiguously assess ipsilateral rVRG axon regrowth, it is critical to perform a complete hemisection.

At fifteen weeks post-C2 hemisection (Fig 1C), the lesion encompassed the entire ventral surface of the spinal cord, extending to the ventral midline (Fig 2A). Transverse spinal cord sections show that the hemisection reached the midline throughout the dorsal-to-ventral extent of the C2 spinal cord (Fig 2B), with ipsilateral degeneration (Fig 2D) and contralateral sparing (Fig 2C) within the ventral horn. Immunostaining of sagittal cervical spinal cord sections with the neuronal marker NeuN demonstrates neuronal survival both rostral and caudal to the injury, but complete neuronal loss throughout the dorsal-to-ventral extent of the lesion site (Fig 2E). We also measured the rostral-caudal width of the lesion (Fig 2F) and found no difference in injury size between animals receiving AAV2-GFP and AAV2-cRheb (Fig 2G). Collectively, these data verify that our hemisection SCI paradigm completely ablated the ipsilateral spinal cord at level C2, while maintaining integrity of the spinal cord immediately rostral and caudal to the lesion, as well as contralateral to the injury site. Furthermore, lesion parameters did not different between experimental groups.

C2 hemisection did not affect functional or morphological innervation of the ipsilateral hemi-diaphragm

We next determined the effect of C2 hemisection on the ipsilateral PhMN pool and on innervation of the hemi-diaphragm. As we performed C2 hemisection rostral to PhMN soma, we expected that PhMN cell body degeneration would not occur and that PhMN innervation of ipsilateral hemi-diaphragm would remain intact. To selectively label PhMN cell bodies, we injected the retrograde tracer, AlexaFluor 555-conjugated cholera toxin B (CTB), via intra-pleural injection into ipsilateral hemi-diaphragm. Following C2 hemisection, the CTB-labeled PhMN pool within the C3-5 spinal cord remained intact in both AAV2-cRheb and AAV2-GFP groups (Fig 3A–B). Additionally, we injected CTB into uninjured laminectomy-only control rats and found no difference in total numbers of CTB-labeled PhMNs (on the side of the injury) between uninjured (58.7 +/− 2.7 PhMNs) and hemisection/AAV2-cRheb (53.7 +/− 4.1 PhMNs) conditions ($p > 0.05$), indicating that the PhMN pool was intact in all groups.

We next examined functional innervation of the ipsilateral hemi-diaphragm by conducting *in vivo* compound muscle action potential (CMAP) recordings in response to supramaximal phrenic nerve stimulation (Fig 3C). We found no differences in peak CMAP amplitudes in the ipsilateral hemi-diaphragm compared to the within-animal contralateral hemi-diaphragm in both AAV2-GFP and AAV2-cRheb groups (Fig 3D). We also found no differences in CMAP amplitudes between AAV2-GFP and AAV2-cRheb in hemi-diaphragm ipsilateral to SCI (Fig 3D).

We then quantitatively assessed morphological innervation of the diaphragm NMJ following C2 hemisection. We labeled ipsilateral hemi-diaphragm in whole-mount preparation with: pan-axonal marker SMI-312 to mark phrenic motor axons, pre-synaptic vesicle marker SV-2 to identify motor axon terminals, and α-bungarotoxin to label post-synaptic nicotinic acetylcholine receptors (Fig 3F–I). Greater than 98% of NMJs were completely intact after C2 hemisection in both AAV2-cRheb and AAV2 GFP animals, with no differences between these two groups in the percentage of fully-innervated, partially-denervated or completely-denervated NMJ (Fig 3J).

Intra-brainstem AAV2 injections specifically transduced neurons within the rVRG

To evaluate the role of Rheb as a neuronal-intrinsic regulator of axonal growth capacity of rVRG neurons, we sought to accurately target neurons within the rVRG. We injected rats with AAV2-GFP or AAV2-mCherry/WGA into the rVRG on one side and sacrificed a cohort of these animals two weeks later to allow adequate time for expression analysis. We observed robust GFP reporter expression within the rVRG, with GFP-labeled cells consistently showing a neuronal morphology (Fig 4A–B). In animals co-injected with both AAV2-GFP and the AAV2-mCherry/WGA tracer, nearly all rVRG cells were co-labeled, indicating that our duel-vector strategy successfully and efficiently transduced rVRG cells with more than one virus simultaneously (Fig 4C). To determine the proportion of the rVRG neuronal population transduced by our AAV2 vectors, we counted the percentage of NeuN+ neurons in the rVRG that co-labeled for the mCherry reporter. We found that greater than 90% of NeuN+ rVRG neurons were mCherry+ (Fig 4D), indicating very high transduction efficiency within the rVRG. To determine the phenotype of transduced cells, we immunostained mCherry-labeled brainstem sections for the astrocyte marker GFAP, the oligodendrocyte lineage marker Olig2 or the neuronal marker NeuN. Representative images show almost no co-localization of GFAP+ and mCherry+ cells (Fig 4F) and little-to-no overlap between Olig2+ and mCherry+ cells (Fig 4G). However, there was almost complete co-localization of NeuN+ and mCherry+ cells, indicating that AAV2 transduction was limited to neurons (Fig 4H). Quantification of this immunostaining showed that >93% of mCherry-labeled cells within the rVRG were NeuN+ neurons, with only a very small percentage of transduced astrocytes or oligodendrocyte lineage cells (Fig 4E). Collectively, these data show that our intra-brainstem injections with AAV2 constructs efficiently targeted neurons within the rVRG.

AAV2-cRheb activated the mTOR pathway within neurons of the rVRG

We next determined the effect of AAV2-cRheb on activation of the mTOR pathway specifically within rVRG neurons. Our AAV2 vector drives expression of HA-tagged cRheb, allowing us to distinguish endogenous and AAV-derived Rheb. At 15 weeks post-SCI, AAV2-cRheb-HA injected animals showed high expression levels of the HA tag within rVRG neurons (Fig 5A). In addition, the HA tag overlapped with mCherry-labeled cells (Fig 5B–C). Ribosomal S6 kinase is downstream of mTOR and is phosphorylated upon mTOR activation; therefore, phosphorylated S6 kinase (pS6K) can be used as a marker for mTOR activation. We quantified the percentage of NeuN+ neurons in the rVRG that co-labeled for pS6K in three groups: (1) laminectomy-only, (2) hemisection + AAV2-GFP, (3) hemisection + AAV2-cRheb. We found no difference in the percentage of rVRG neurons that co-labeled with pS6K; 100% of rVRG neurons in all three groups were pS6K-positive. Additionally, we quantified pS6K expression levels in rVRG neurons. Compared to AAV2-GFP control (Fig 5D), AAV2-cRheb-HA injection (Fig 5E) induced an approximately three-fold increase in pS6K levels in NeuN+ rVRG cells at 15 weeks post-SCI (Fig 5F), as well as an approximately two-fold increase over laminectomy-only uninjured controls, indicating that the mTOR pathway was significantly activated in rVRG neurons upon cRheb expression.

AAV2-cRheb expression induced rVRG axonal regeneration

Our findings demonstrate that intra-brainstem injection of AAV-cRheb vector selectively, efficiently and persistently transduced rVRG neurons in rats receiving C2 hemisection SCI and that cRheb expression significantly stimulated mTOR pathway activation in these rVRG neurons. Therefore, we sought to determine whether AAV2-cRheb would promote regeneration of injured rVRG axons after cervical SCI. To address this question, we co-injected AAV2-mCherry/WGA along with AAV2-GFP or AAV2-cRheb into rVRG ipsilateral to the hemisection. At fifteen weeks post-SCI (thirteen weeks post-rVRG injection), we quantified mCherry+ rVRG fibers in sagittal spinal cord sections at various rostral-caudal distances relative to the lesion site. Specifically, we used the border of the lesion site and intact rostral spinal cord as the starting point. We quantified the number of mCherry-labeled rVRG axons rostral and caudal to this starting point, counting every fiber in 100 micron-wide rostral-caudal bins, diagramed in Fig. 6A. In the AAV2-GFP group, there was substantial axon die-back into the intact rostral spinal cord. AAV2-cRheb significantly reduced rVRG fiber die-back at several distances rostral to the lesion compared to AAV2-GFP. At even greater rostral distances, rVRG axon counts were eventually not different between GFP and cRheb conditions. Excitingly, while there were no mCherry+ axons at all within the lesion in the AAV2-GFP group, AAV2-cRheb promoted regeneration of injured rVRG axons into the lesion. Despite this regeneration, no rVRG fibers crossed all the way through the lesion and back into intact caudal tissue (Fig 6B). Representative images of spinal cord 1 mm rostral to the lesion site show similar mCherry labeling between the two groups (Fig C–D). In the intact spinal cord just rostral to the lesion, there were significantly more mCherry-labeled rVRG axons in AAV2-cRheb rats (Fig 6F) compared to AAV2-GFP (Fig 6E). In addition, no mCherry+ axons were observed growing into the lesion with AAV2-GFP (Fig 6E), while rVRG axons regenerated across the intact-lesion interface with cRheb expression (Fig 6F). At the lesion center (up to 300μm from the intact-lesion border), we also observed regeneration of rVRG fibers with AAV2-cRheb (Fig 6H), but none in AAV2-GFP animals (Fig 6G).

In addition to regeneration, cRheb expression could exert effects on sprouting of these rVRG axons into, for example, contralateral intact spinal cord. Following AAV2-mCherry injection into rVRG ipsilateral to the hemisection, we found no mCherry-labeled fibers in contralateral spinal cord rostral or caudal to the injury (data not shown).

We additionally examined synapse formation between rVRG axons and PhMNs within the C3 level of the spinal cord in both uninjured and C2 hemisected animals. We observed robust co-localization of mCherry-labeled rVRG fibers with vGlut2-positive excitatory pre-synaptic terminals and CTB-labeled PhMNs in uninjured animals, showing synaptic connections between rVRG axons and all PhMNs (Fig 6I–L). In addition, we found accumulation of the trans-synaptic tracer WGA in CTB-labeled PhMNs in these uninjured animals following injection of AAV2-mCherry/WGA into ipsilateral rVRG (Fig 6M–P). However, no mCherry-labeled rVRG fibers were located caudal to the lesion at the C3-5 levels in C2 hemisection animals that received AAV2-GFP or AAV2-cRheb (data not shown). These findings demonstrate that, despite regeneration of injured rVRG axons into

the lesion site, these fibers did not re-enter caudal intact spinal cord to reinnervate their PhMN targets.

AAV2-cRheb transduction of rVRG neurons did not promote recovery of diaphragm function following C2 hemisection

Lastly, we examined whether cRheb expression in injured rVRG neurons resulted in ipsilateral hemi-diaphragm recovery. We quantitatively tested diaphragm function *in vivo* by electromyography (EMG) at 14 weeks post-SCI. Furthermore, given that different sub-regions of the hemi-diaphragm are innervated by PhMN soma located at different portions of the C3-5 spinal cord, we conducted EMG recordings separately at dorsal, medial and ventral diaphragm. Compared to uninjured control rats (Fig 7A), both AAV2-GFP (Fig 7B) and AAV2-cRheb (Fig 7C) groups showed significantly reduced amplitudes of inspiratory bursts. The hemi-diaphragm was near-silent in these SCI animals; only 10-20% of pre-injury amplitude remained, which was likely due to the small amount of spontaneous recovery normally observed after C2 hemisection (which is driven by spared contralateral input). There were no differences between AAV2-cRheb and AAV2-GFP in burst amplitude (Fig 7D), duration (data not shown) or frequency (data not shown) at any of the three ipsilateral hemi-diaphragm sub-regions. These functional data indicate that, while cRheb expression promoted rVRG regeneration, it did not promote recovery of diaphragmatic respiratory function.

Discussion

We have shown that expression of cRheb selectively in rVRG neurons following cervical hemisection SCI stimulates mTOR pathway activation within transduced cells, reduces dieback of injured rVRG fibers and, importantly, promotes regeneration of this critical population of bulbospinal respiratory axons.

We established a set of experimental tools to histopathologically assess rVRG-PhMN-diaphragm circuitry, including rVRG cell bodies in the brainstem, descending rVRG axonal projections within cervical spinal cord, rVRG synaptic input to PhMNs, and PhMN innervation at the diaphragm NMJ. Of note, we demonstrated that our novel AAV2-mCherry/WGA vector allows for the assessment of monosynaptic connectivity between descending rVRG axons and PhMNs that are selectively labeled from the diaphragm with CTB. Going forward, these circuit tracing methods can be used in conjunction with C2 hemisection and cervical contusion SCI models to comprehensively study plasticity of the critical rVRG-PhMN-diaphragm pathway that is central to the control of diaphragm activation.

Despite these exciting findings of rVRG axon regeneration in response to cRheb expression, regrowth did not occur back into the intact caudal spinal cord to establish synaptic reinnervation of PhMNs. Furthermore, trans-synaptic WGA labeling was absent from ipsilateral CTB-labeled PhMNs in hemisection animals receiving AAV2-cRheb, demonstrating that no rVRG axons were able to synapse back onto their targets. Given that we observed no effects of cRheb on diaphragm EMG amplitudes, our findings suggest that re-establishment of direct rVRG-PhMN connectivity is important (and possibly necessary)

for promoting recovery of diaphragm function after cervical SCI. Importantly, the rVRG-PhMN-diaphragm pathway provides an ideal model system with which to study regeneration and circuit reconnection for several key reasons: (1) neuroanatomical control of diaphragm activation is well-defined; (2) damage to this circuit is centrally important to cervical SCI patients; (3) a battery of *in vivo* functional, electrophysiological and neuronal tracing methods are available to assess this circuitry in cervical SCI models. This paradigm and set of experimental tools will be valuable for the SCI field for testing strategies to promote circuit reconstruction and to mechanistically evaluate the contribution of various modes of axonal plasticity (e.g. regeneration, sprouting) to functional improvement.

Our data suggest that manipulation of additional factors that limit axonal growth will also be necessary to coax regrowing rVRG axons back into the distal intact spinal cord to reconstruct damaged rVRG-PhMN circuitry. Strategies to address this issue could include blocking the neuronal-extrinsic inhibitory effects of chondroitin sulfate proteoglycans (CSPGs) (Cregg et al., 2014). Indeed, our data are in line with previous studies from the laboratory of Veronica Tom demonstrating that expression of cRheb stimulates regeneration of propriospinal axons, primary afferent sensory fibers and descending axons after T7 transection, dorsal root crush and C2 hemisection injuries, respectively, when combined with CSPGs modulation (Wu et al., 2015; Wu et al., 2016; Wu et al., 2017). In agreement with their findings, we observed axonal regrowth of cRheb-expressing neurons into the lesion site, indicating that cRheb alone has the capacity to increase the intrinsic growth capacity of CNS neurons post-SCI. In their experiments, they found that the combination of AAV-cRheb vector, a peripheral nerve graft and treatment with chondroitinase ABC (chABC) induces regenerating axons to reenter distal spinal cord. A similar strategy may be relevant to promoting PhMN reinnervation by regenerating rVRG axons following cervical SCI.

Our study indicates that activation of neuronal-intrinsic, pro-growth pathways leads to rVRG axon regeneration after SCI. However, this regrowth response is only limited with cRheb expression, as axons do not exit the lesion site to re-enter intact distal spinal cord. These data suggest that activation of the mTOR pathway alone may be insufficient to produce robust growth after CNS damage. Interestingly, genetic co-deletion of PTEN and suppressor of cytokine signaling 3 (SOCS3) (Sun et al., 2011) produces significant and, importantly, sustained corticospinal tract axon regeneration after CNS injury, suggesting that modulation of multiple neuronal-intrinsic signaling pathways may be necessary to both (1) activate an rVRG growth state and (2) maintain this response to allow extension over necessary distances (i.e. for sufficient temporal duration) to achieve reinnervation of PMNs up to several segments from the lesion site.

Compared to previous axon growth studies that manipulated PTEN signaling using genetic deletion (Liu et al., 2010; Park et al., 2008; Willenberg et al., 2016) or viral vector-based shRNA knockdown (Lewandowski and Steward, 2014; Zukor et al., 2013), we observe a less robust effect on rVRG axon regeneration with cRheb expression; several reasons may potentially explain these differences. Unlike with knockout/knockdown of PTEN expression, cRheb stimulation of S6 kinase 1 may induce feedback inhibition of the phosphatidylinositol 3-kinase/mTOR signaling axis (Al-Ali et al., 2017), while inhibition of PTEN at the “top” of the pathway may avoid this effect. In addition, PTEN knockdown could be affecting

multiple signaling pathways regulating axon regeneration (Park et al., 2010), while we are only targeting downstream targets of Rheb by expressing constitutively-active Rheb. Furthermore, axonal growth after SCI (including in response to PTEN deletion) decreases significantly with age (Geoffroy et al., 2016) and time point post-axotomy (Steinmetz et al., 2005; Ylera et al., 2009). In our experimental paradigm, we waited 7 days following C2 hemisection SCI to inject AAV2-cRheb into the rVRG, as we sought to test a more clinically-translatable time point. We have also found that it takes 10-14 days post-AAV2 injection to achieve efficient rVRG neuron transduction and gene expression (data not shown). Therefore, we are not likely achieving robust cRheb expression until 2-3 weeks post-SCI, which may coincide temporally with a point when rVRG axons have reduced responsiveness to driving the Rheb-mTOR pathway. Conversely, previous work with PTEN deletion was typically conducted with genetic knockout in an inducible manner prior to even generating the injury.

Regeneration of damaged axons and synaptic reconnection with original neuronal targets represents only one mode of axonal plasticity that may be capable of driving respiratory recovery after SCI. Other mechanisms include sprouting of spared rVRG fibers (originating in the contralateral rVRG in the hemisection model) to reinnervate PhMNs (Boulenguez et al., 2007; Goshgarian, 2009) and growth of descending serotonergic axons that play an important role in regulating the excitability of PhMNs (Mantilla et al., 2012; Mitchell et al., 1992; Zhou et al., 2001). In the current study, we used a targeted viral delivery approach to selectively stimulate Rheb signaling in only ipsilateral rVRG neurons; therefore, we were unable to investigate the effects of activating the Rheb-mTOR pathway in these other supraspinal neuronal populations that are involved in diaphragmatic respiratory drive. Nevertheless, our data demonstrate that cRheb expression does promote growth effects on rVRG axons, suggesting that less directed strategies such as pharmacological agents to target the PTEN-Rheb-mTOR axis may be able to promote diaphragmatic recovery by simultaneously affecting multiple descending inputs to the PhMN pool.

Previous work suggests that axonal growth within SCI lesion sites often occurs along astrocyte “bridges” (Zukor et al., 2013; Zukor et al., 2011), while resident microglial-derived and peripheral hematogenous monocyte-derived macrophages prevent axonal extension and induce profound axonal die-back (Silver et al., 2014). We did not find that rVRG axons selectively avoided areas with ED1+ macrophages. We found that the entire core of the lesion site was fairly uniformly filled with ED1+ cells, so we did not observe areas devoid of macrophages; therefore, we could not detect any preference for the growth trajectory of regenerating rVRG axons with respect to macrophage location (data not shown). We also did not find that rVRG axons preferentially extended along the processes of GFAP+ astrocytes or conversely that they avoided these astrocytes (data not shown). It will be important in future work to determine the neuronal-extrinsic mechanisms involved in rVRG axon regeneration in response to Rheb pathway activation.

In conclusion, these exciting results demonstrate that modulation of signaling pathways that regulate axon growth potential within defined populations of supraspinal respiratory neurons can promote axon regeneration. Optimizing this effect to achieve reconnection of the critical

rVRG-PhMN circuitry that controls diaphragm function will have profound implication for individuals suffering from debilitating respiratory compromise after cervical SCI.

Acknowledgments

This work was supported by the Craig H. Neilsen Foundation (grant #476686 to A.C.L.) and the NINDS (grant #1R01NS079702 to A.C.L.).

Abbreviations

AAV2	adeno-associated virus serotype-2
C2 (3, 4, 5, etc.)	cervical spinal cord level 2 (3, 4, 5, etc.)
CMAP	compound muscle action potential
CNS	central nervous system
CTB	cholera toxin subunit B
EMG	electromyography
GAP	GTPase-activating protein
HA	hemagglutinin tag
mTOR	mechanistic target of rapamycin
NMJ	neuromuscular junction
PhMN	phrenic motor neuron
pS6k	phosphorylated ribosomal S6 kinase
PTEN	phosphatase and tensin homolog
rVRG	rostral ventral respiratory group
Rheb	ras homolog enriched in brain
cRheb	constitutively-active Rheb
SCI	spinal cord injury
TSC1/2	tumor sclerosis complex protein 1/2

References

Al-Ali H, Ding Y, Slepak T, Wu W, Sun Y, Martinez Y, Xu XM, Lemmon VP, Bixby JL. The mTOR substrate S6 Kinase 1 (S6K1) is a negative regulator of axon regeneration and a potential drug target for Central Nervous System injury. J Neurosci. 2017; 37(30):7079–7095. [PubMed: 28626016]

Alilain WJ, Horn KP, Hu H, Dick TE, Silver J. Functional regeneration of respiratory pathways after spinal cord injury. Nature. 2011; 475(7355):196–200. [PubMed: 21753849]

Boulenguez P, Gauthier P, Kastner A. Respiratory neuron subpopulations and pathways potentially involved in the reactivation of phrenic motoneurons after C2 hemisection. Brain Res. 2007; 1148:96–104. [PubMed: 17379194]

Busch SA, Silver J. The role of extracellular matrix in CNS regeneration. Curr Opin Neurobiol. 2007; 17(1):120–127. [PubMed: 17223033]

Cafferty WB, McGee AW, Strittmatter SM. Axonal growth therapeutics: regeneration or sprouting or plasticity? Trends Neurosci. 2008; 31(5):215–220. [PubMed: 18395807]

Cregg JM, DePaul MA, Filous AR, Lang BT, Tran A, Silver J. Functional regeneration beyond the glial scar. Exp Neurol. 2014; 253:197–207. [PubMed: 24424280]

Danilov CA, Steward O. Conditional genetic deletion of PTEN after a spinal cord injury enhances regenerative growth of CST axons and motor function recovery in mice. Exp Neurol. 2015; 266:147–160. [PubMed: 25704959]

Dell'Anno MT, Strittmatter SM. Rewiring the spinal cord: Direct and indirect strategies. Neurosci Lett. 2017; 652:25–34. [PubMed: 28007647]

Dobbins GD, Feldman JL. Brainstem Network Controlling Descending Drive to Phrenic Motoneurons in Rat. J Comp Neurol. 1994; 347(1):64–86. [PubMed: 7798382]

Durán RV, Hall MN. Regulation of TOR by small GTPases. EMBO Rep. 2012; 13(2):121–128. [PubMed: 22240970]

Fitch MT, Silver J. CNS injury, glial scars, and inflammation: Inhibitory extracellular matrices and regeneration failure. Exp Neurol. 2008; 209(2):294–301. [PubMed: 17617407]

Geoffroy CG, Hilton BJ, Tetzlaff W, Zheng B. Evidence for an Age-Dependent Decline in Axon Regeneration in the Adult Mammalian Central Nervous System. Cell Rep. 2016; 15(2):238–246. [PubMed: 27050519]

Gervasi NM, Kwok JC, Fawcett JW. Role of extracellular factors in axon regeneration in the CNS: implications for therapy. Regen Med. 2008; 3(6):907–923. [PubMed: 18947312]

Ghali MGZ. The bulbospinal network controlling the phrenic motor system: Laterality and course of descending projections. Neurosci Res. 2017; 121:7–17. [PubMed: 28389264]

Goshgarian HG. The crossed phrenic phenomenon and recovery of function following spinal cord injury. Respir Physiol Neurobiol. 2009; 169(2):85–93. [PubMed: 19539790]

Gutilla EA, Steward O. Selective neuronal PTEN deletion: can we take the brakes off of growth without losing control. Neural Regen Res. 2016; 11(8):1201–1203. [PubMed: 27651754]

Harel NY, Strittmatter SM. Can regenerating axons recapitulate developmental guidance during recovery from spinal cord injury. Nat Rev Neurosci. 2006; 7(8):603–616. [PubMed: 16858389]

Lewandowski G, Steward O. AAVshRNA-Mediated Suppression of PTEN in Adult Rats in Combination with Salmon Fibrin Administration Enables Regenerative Growth of Corticospinal Axons and Enhances Recovery of Voluntary Motor Function after Cervical Spinal Cord Injury. J Neurosci. 2014; 34(30)

Lipski J, Zhang X, Kruszewska B, Kanjhan R. Morphological study of long axonal projections of ventral medullary inspiratory neurons in the rat. Brain Res. 1994; 640(1–2):171–184. [PubMed: 8004446]

Liu K, Lu Y, Lee JK, Samara R, Willenberg R, Sears-Kraxberger I, Tedeschi A, Park KK, Jin D, Cai B, Xu B, Connolly L, Steward O, Zheng B, He Z. PTEN deletion enhances the regenerative ability of adult corticospinal neurons. Nat Neurosci. 2010; 13(9):1075–1081. [PubMed: 20694004]

Long X, Lin Y, Ortiz-Vega S, Yonezawa K, Avruch J. Rheb binds and regulates the mTOR kinase. Curr Biol. 2005; 15(8):702–713. [PubMed: 15854902]

Lu Y, Belin S, He Z. Signaling regulations of neuronal regenerative ability. Curr Opin Neurobiol. 2014; 27:135–142. [PubMed: 24727245]

Mantilla CB. Gene therapy and respiratory neuroplasticity. Exp Neurol. 2017; 287(Pt 2):261–267. [PubMed: 27697480]

Mantilla CB, Bailey JP, Zhan WZ, Sieck GC. Phrenic motoneuron expression of serotonergic and glutamatergic receptors following upper cervical spinal cord injury. Exp Neurol. 2012; 234(1): 191–199. [PubMed: 22227062]

Mitchell GS, Sloan HE, Jiang C, Miletic V, Hayashi F, Lipski J. 5-Hydroxytryptophan (5-HTP) augments spontaneous and evoked phrenic motoneuron discharge in spinalized rats. Neurosci Lett. 1992; 141(1):75–78. [PubMed: 1508404]

Nicaise C, Hala TJ, Frank DM, Parker JL, Authelet M, Leroy K, Brion JP, Wright MC, Lepore AC. Phrenic motor neuron degeneration compromises phrenic axonal circuitry and diaphragm activity in a unilateral cervical contusion model of spinal cord injury. Exp Neurol. 2012a; 235(2):539–552. [PubMed: 22465264]

Nicaise C, Putatunda R, Hala TJ, Regan KA, Frank DM, Brion JP, Leroy K, Pochet R, Wright MC, Lepore AC. Degeneration of phrenic motor neurons induces long-term diaphragm deficits following midcervical spinal contusion in mice. J Neurotrauma. 2012b; 29(18):2748–2760. [PubMed: 23176637]

Ohtake Y, Hayat U, Li S. PTEN inhibition and axon regeneration and neural repair. Neural Regen Res. 2015; 10(9):1363–1368. [PubMed: 26604880]

Park KK, Liu K, Hu Y, Kanter JL, He Z. PTEN/mTOR and axon regeneration. Exp Neurol. 2010; 223(1):45–50. [PubMed: 20079353]

Park KK, Liu K, Hu Y, Smith PD, Wang C, Cai B, Xu B, Connolly L, Kramvis I, Sahin M, He Z. Promoting axon regeneration in the adult CNS by modulation of the PTEN/mTOR pathway. Science. 2008; 322(5903):963–966. [PubMed: 18988856]

Ribas VT, Costa MR. Gene Manipulation Strategies to Identify Molecular Regulators of Axon Regeneration in the Central Nervous System. Front Cell Neurosci. 2017; 11:231. [PubMed: 28824380]

Silver J, Schwab ME, Popovich PG. Central nervous system regenerative failure: role of oligodendrocytes, astrocytes, and microglia. Cold Spring Harb Perspect Biol. 2014; 7(3)

Steinmetz MP, Horn KP, Tom VJ, Miller JH, Busch SA, Nair D, Silver DJ, Silver J. Chronic enhancement of the intrinsic growth capacity of sensory neurons combined with the degradation of inhibitory proteoglycans allows functional regeneration of sensory axons through the dorsal root entry zone in the mammalian spinal cord. J Neurosci. 2005; 25(35):8066–8076. [PubMed: 16135764]

Sun F, Park KK, Belin S, Wang D, Lu T, Chen G, Zhang K, Yeung C, Feng G, Yankner BA, He Z. Sustained axon regeneration induced by co-deletion of PTEN and SOCS3. Nature. 2011; 480(7377):372–375. [PubMed: 22056987]

University of Alabama, Birmingham. The National Spinal Cord Injury Statistical Center, 2016. Annual Statistical Reports. 2016

Vinit S, Gauthier P, Stamegna JC, Kastner A. High cervical lateral spinal cord injury results in long-term ipsilateral hemidiaphragm paralysis. J Neurotrauma. 2006; 23(7):1137–1146. [PubMed: 16866626]

Vinit S, Kastner A. Descending bulbospinal pathways and recovery of respiratory motor function following spinal cord injury. Respir Physiol Neurobiol. 2009; 169(2):115–122. [PubMed: 19682608]

Willenberg R, Zukor K, Liu K, He Z, Steward O. Variable laterality of corticospinal tract axons that regenerate after spinal cord injury as a result of PTEN deletion or knock-down. J Comp Neurol. 2016; 524(13):2654–2676. [PubMed: 26878190]

Wright MC, Son YJ. Ciliary neurotrophic factor is not required for terminal sprouting and compensatory reinnervation of neuromuscular synapses: re-evaluation of CNTF null mice. Exp Neurol. 2007; 205(2):437–448. [PubMed: 17445802]

Wu D, Klaw MC, Connors T, Kholodilov N, Burke RE, Tom VJ. Expressing Constitutively Active Rheb in Adult Neurons after a Complete Spinal Cord Injury Enhances Axonal Regeneration beyond a Chondroitinase-Treated Glial Scar. J Neurosci. 2015; 35(31):11068–11080. [PubMed: 26245968]

Wu D, Klaw MC, Kholodilov N, Burke RE, Detloff MR, Côté MP, Tom VJ. Expressing Constitutively Active Rheb in Adult Dorsal Root Ganglion Neurons Enhances the Integration of Sensory Axons that Regenerate Across a Chondroitinase-Treated Dorsal Root Entry Zone Following Dorsal Root Crush. Front Mol Neurosci. 2016; 9:49. [PubMed: 27458339]

Wu D, K MC, Connors T, Kholodilov N, Burke RE, Côté MP, Tom VJ. Combining Constitutively Active Rheb Expression and Chondroitinase Promotes Functional Axonal Regeneration after Cervical Spinal Cord Injury. Mol Ther. 2017; 25(12):2715–2726. [PubMed: 28967557]

Yiu G, He Z. Glial inhibition of CNS axon regeneration. Nat Rev Neurosci. 2006; 7(8):617–627. [PubMed: 16858390]

Ylera B, Ertürk A, Hellal F, Nadrigny F, Hurtado A, Tahirovic S, Oudega M, Kirchhoff F, Bradke F. Chronically CNS-injured adult sensory neurons gain regenerative competence upon a lesion of their peripheral axon. Curr Biol. 2009; 19(11):930–936. [PubMed: 19409789]

Zhang Y, Gao X, Saucedo LJ, Ru B, Edgar BA, Pan D. Rheb is a direct target of the tuberous sclerosis tumour suppressor proteins. Nat Cell Biol. 2003; 5(6):578–581. [PubMed: 12771962]

Zhou SY, Basura GJ, Goshgarian HG. Serotonin(2) receptors mediate respiratory recovery after cervical spinal cord hemisection in adult rats. J Appl Physiol. 2001; 91(6):2665–2673. [PubMed: 11717232]

Zukor K, Belin S, Wang C, Keelan N, Wang X, He Z. Short hairpin RNA against PTEN enhances regenerative growth of corticospinal tract axons after spinal cord injury. J Neurosci. 2013; 33(39): 15350–15361. [PubMed: 24068802]

Zukor KA, Kent DT, Odelberg SJ. Meningeal cells and glia establish a permissive environment for axon regeneration after spinal cord injury in newts. Neural Dev. 2011; 6:1. [PubMed: 21205291]

Highlights

- Constitutively-active Rheb promotes regeneration of bulbospinal rVRG axons after SCI
- cRheb expression also reduces dieback of injured rVRG axons following cervical SCI
- cRheb expression stimulates mTOR pathway activity within transduced rVRG neurons
- Regenerating rVRG axons do not extend back to caudal spinal cord to reinnervate PhMNs
- cRheb alone does not promote recovery of diaphragmatic respiratory function after SCI

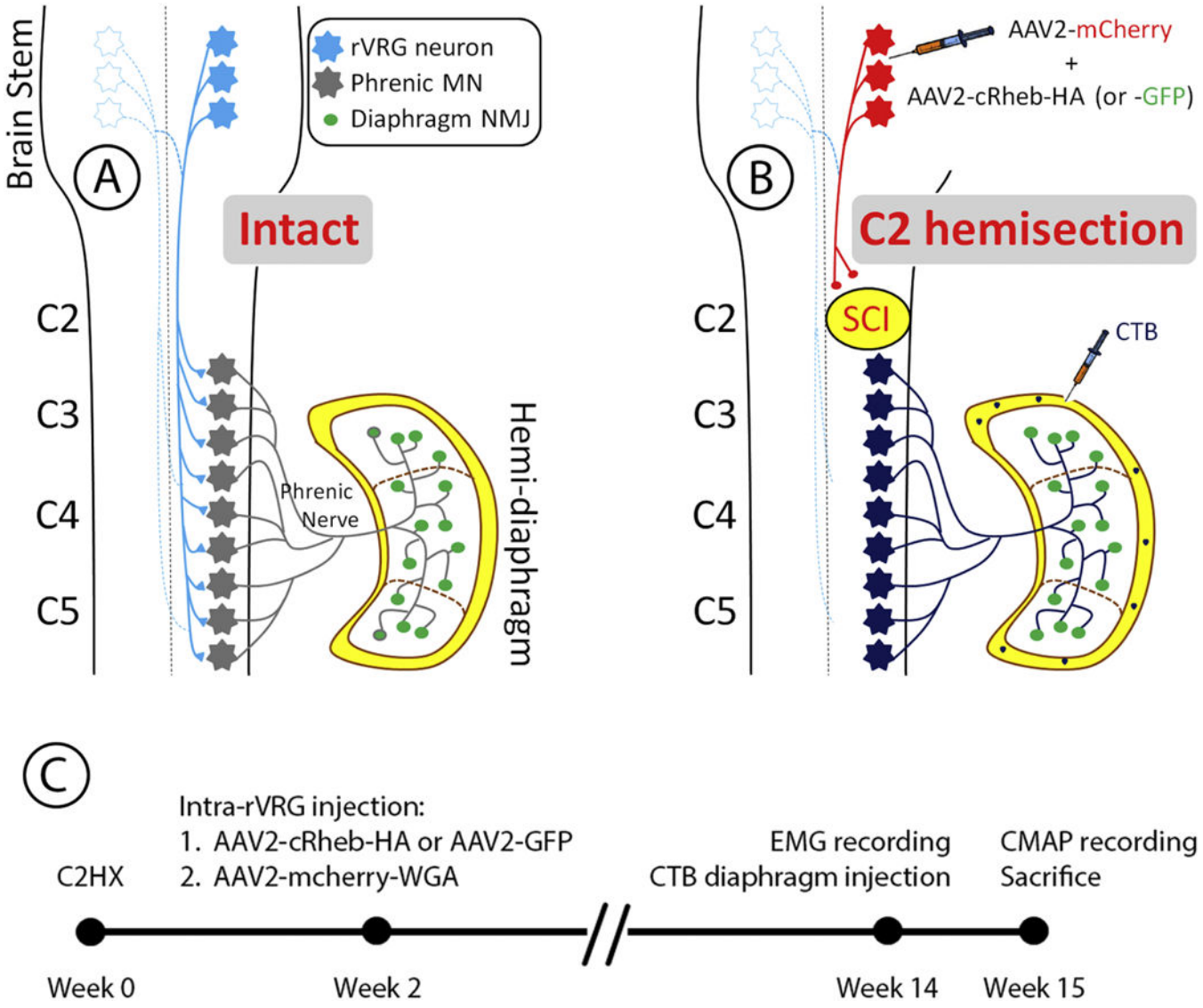

Figure 1. Schematic of rVRG-PhMN-diaphragm circuit

Diagram depicting intact circuit (**A**). Experimental procedure and effects of C2 hemisection on circuit (**B**). (**C**) Experimental timeline: We administered C2 hemisection (C2HX), ablating connection from rVRG to ipsilateral PhMNs. We transduced rVRG neurons with AAV2-mCherry and either AAV2-cRheb-HA or AAV2-GFP at 2 weeks post-hemisection. At 14 weeks post-SCI, we performed EMG recordings and injected CTB into the ipsilateral hemi-diaphragm. At 15 weeks, we performed CMAP recordings and sacrificed animals.

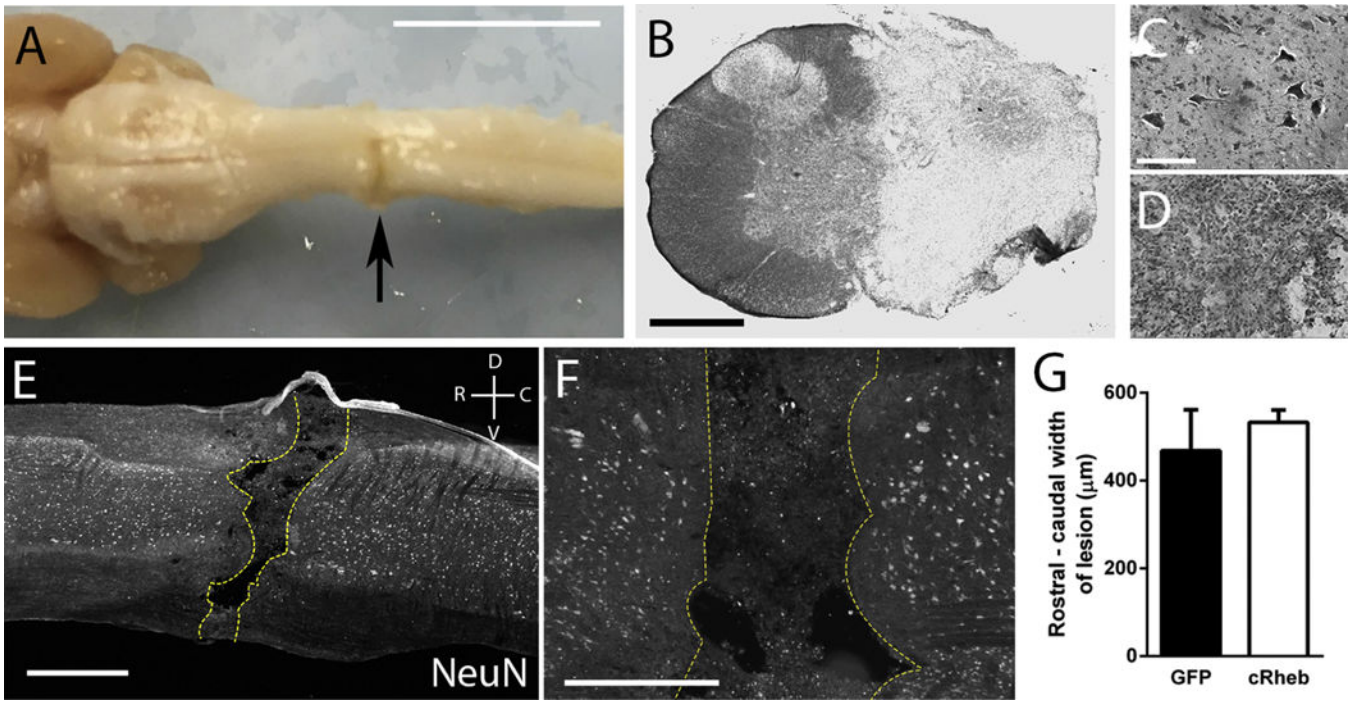

Figure 2. C2 hemisection completely disrupted ipsilateral hemi-spinal cord

At 15 weeks post-C2 hemisection, the lesion encompassed the entire ventral surface of the spinal cord, extending to the ventral midline (**A**); scale bar: 1 mm. Transverse spinal cord sections show that the hemisection reached the midline throughout the dorsal-to-ventral extent of the C2 spinal cord (**B**); scale bar: 660 μm. Higher magnification images show ipsilateral neuronal degeneration (**D**) and contralateral sparing (**C**) within the ventral horn; scale bar: 200 μm. Immunostaining of sagittal cervical spinal cord sections with the neuronal marker NeuN demonstrates neuronal survival both rostral and caudal to the injury, but complete neuronal loss throughout the dorsal-to-ventral extent of the lesion site (**E**-**F**); scale bar in E: 1 mm; scale bar in F: 500 μm. Dotted yellow lines in E-F denote the injury border. There was no difference in the rostral-caudal width of the lesion between animals receiving AAV2-GFP and AAV2-cRheb (**G**): n = 3 per group, 3 tissue sections per animal, 5 equidistant lengths per lesion measured starting at the dorsal end of the section.

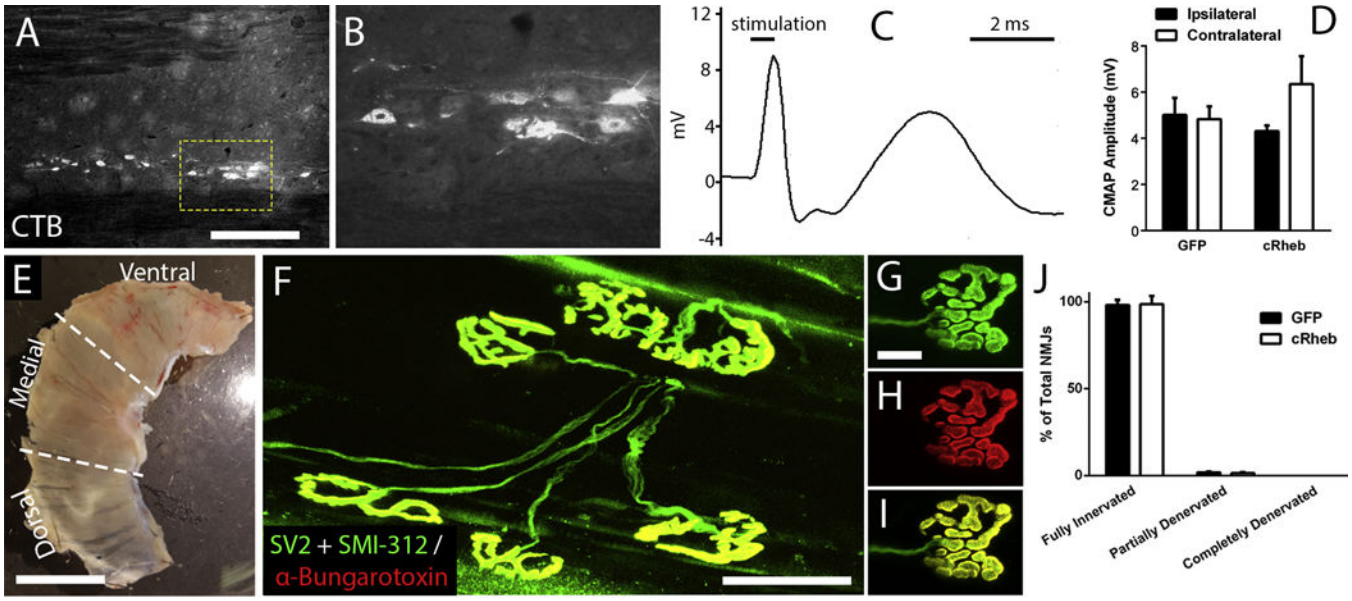

Figure 3. C2 hemisection did not affect functional or morphological innervation of the ipsilateral hemi-diaphragm

To selectively label PhMN soma, we injected the retrograde tracer, AlexaFluor 555-conjugated cholera toxin B (CTB), via intra-pleural injection into ipsilateral hemi-diaphragm. Following C2 hemisection, the CTB-labeled PhMN pool within the C3-5 spinal cord remained intact, as shown in sagittal spinal cord sections (**A**-**B**). Scale bar: 450 μm (A), 100 μm (B). There were no differences in peak compound muscle action potential (CMAP) amplitudes in the ipsilateral hemi-diaphragm (representative trace shown in **C**) compared to the within-animal contralateral hemi-diaphragm in both AAV2-GFP and AAV2-cRheb groups (**D**). No differences were found in CMAP amplitudes between AAV2-GFP and AAV2-cRheb in hemi-diaphragm ipsilateral to SCI (**D**). Image depicts dorsal, medial and ventral sub-regions of the hemi-diaphragm (**E**); scale bar: 1 cm. Diaphragms were labeled with anti-SV2, anti-SMI-312 and α-bungarotoxin for NMJ morphology analysis. Representative images of diaphragm NMJ: SMI-312 + SV2 (**G**), α-bungarotoxin (**H**), overlap (**F**, **I**). Scale bar: 100 μm (F), 50 μm (G-I). Greater than 98% of NMJs in the ipsilateral hemi-diaphragm were completely intact after C2 hemisection in both AAV2-cRheb and AAV2 GFP animals, with no differences between these two groups in the percentage of fully-innervated, partially-denervated or completely-denervated NMJ (**J**).

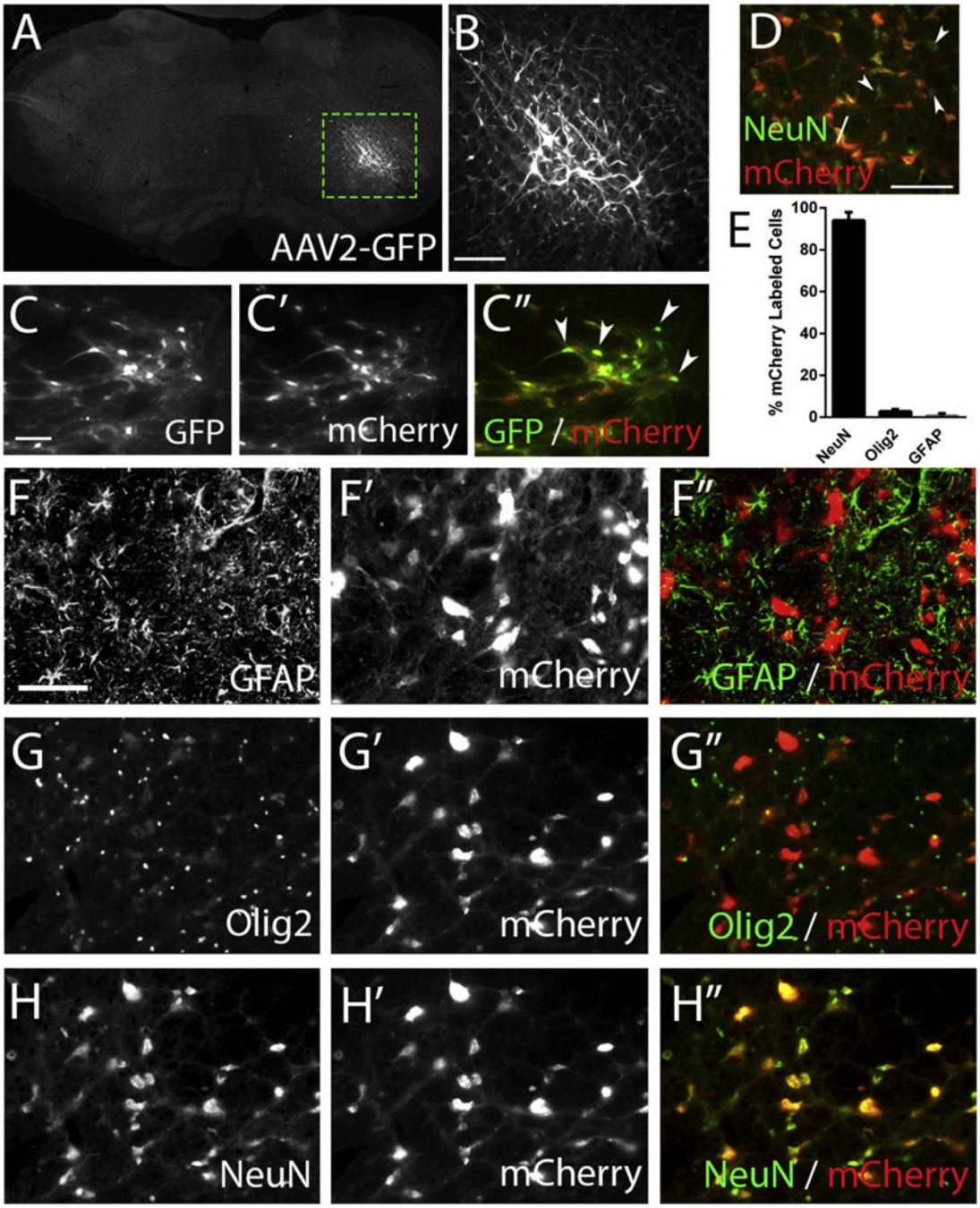

Figure 4. Intra-brainstem AAV2 injections specifically transduced neurons within the rVRG

We injected rats with AAV2-GFP or AAV2-mCherry into the rVRG and sacrificed these animals two weeks later. We observed robust GFP reporter expression within the rVRG, with GFP-labeled cells consistently showing a neuronal morphology (**A**); scale bar: 500 μm. The dotted box in **A** outlines the higher magnification image shown in (**B**); scale bar: 100 μm. In animals coinjected with both AAV2-GFP and the AAV2-mCherry tracer, nearly all rVRG cells were co-labeled (**C**, **C′**, **C″**); scale bar: 100 μm; white arrowheads indicate representative neurons that express both reporters. Transduction efficiency was greater than

90%, as assessed by quantifying the percentage of NeuN+ neurons in the rVRG that co-labeled for the mCherry reporter; white arrowheads indicate NeuN+ cells not labeled with mCherry (**D**); scale bar: 100 μm. Representative images show almost no co-localization of GFAP+ astrocytes and mCherry+ cells (**F**, **F′**, **F″**) and little overlap between Olig2+ oligodendrocyte lineage cells and mCherry+ cells (**G**, **G′**, **G″**); scale bar: 100 μm. However, there was almost complete co-localization of NeuN+ neurons and mCherry+ cells (**H**, **H′**, **H″**). Quantification showed that >93% of mCherry-labeled cells within the rVRG were NeuN+ neurons, with < 5% of either transduced astrocytes or oligodendrocyte lineage cells (**E**).

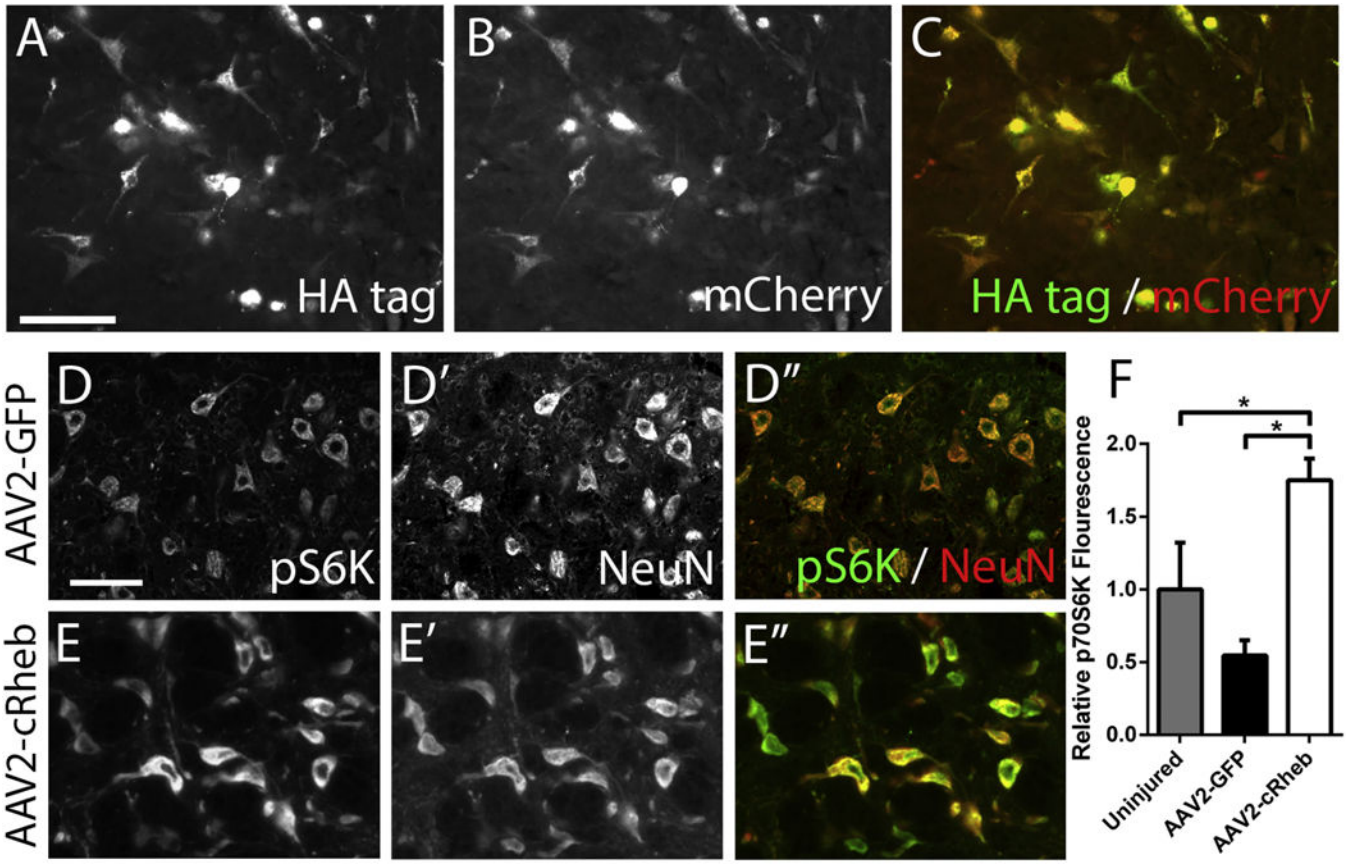

Figure 5. AAV2-cRheb activated the mTOR pathway within neurons of the rVRG

At 15 weeks post-SCI, AAV2-cRheb-HA injected animals showed high expression levels of the HA tag within rVRG neurons (**A**). In addition, the HA tag overlapped with mCherry-labeled cells (**B**-**C**); scale bar: 100 μm. Compared to AAV2-GFP control (**D**, **D′**, **D″**), AAV2-cRheb-HA injection (**E**, **E′**, **E″**) induced an approximately three-fold increase in pS6K levels in NeuN+ rVRG cells at 15 weeks post-SCI, as well as a significant increase over laminectomy-only uninjured control (**F**), scale bar: 100 μm.

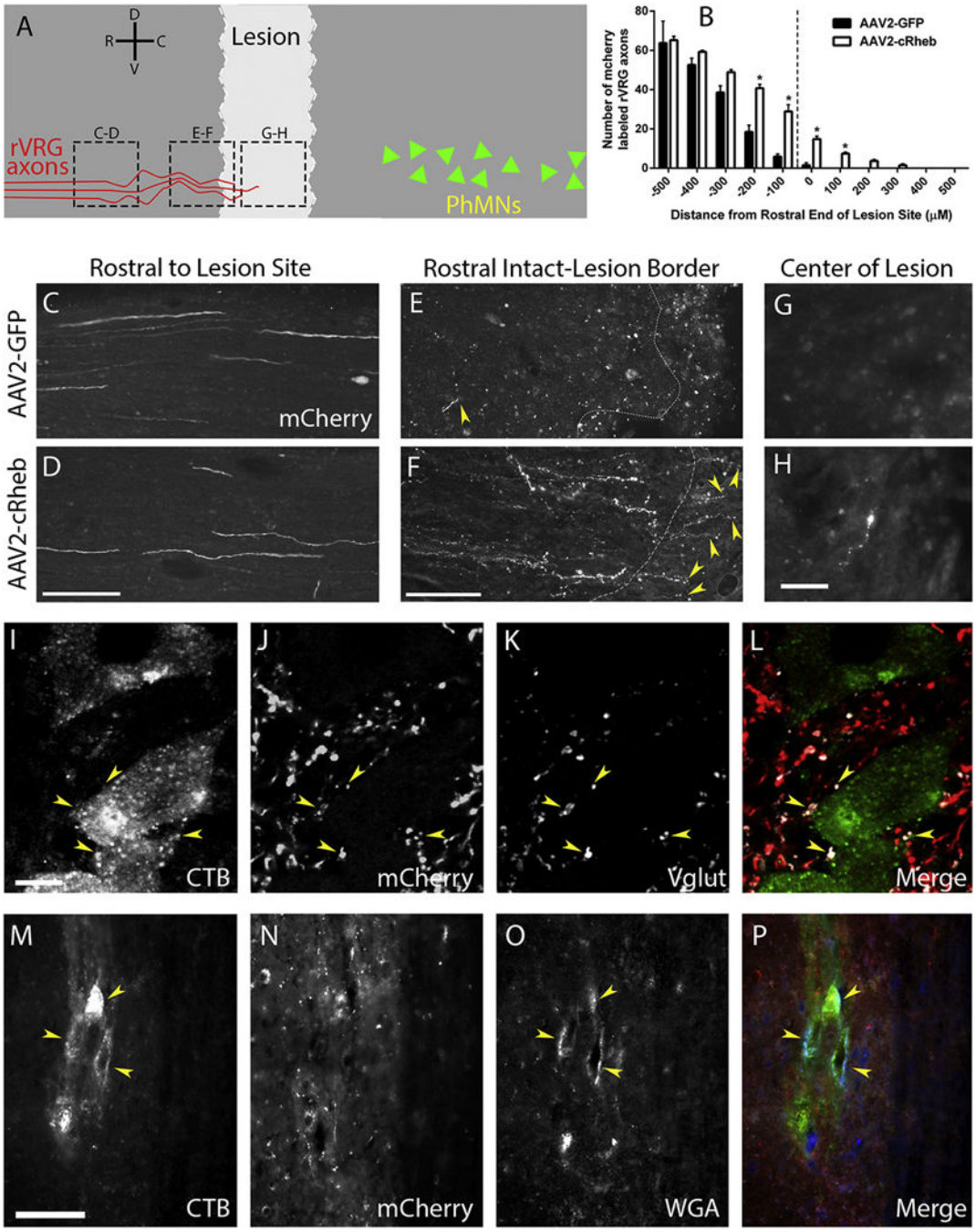

Figure 6. AAV2-cRheb expression induced rVRG axonal regeneration

We co-injected AAV2-mCherry along with AAV2-GFP or AAV2-cRheb into rVRG ipsilateral to C2 hemisection. At 15 weeks post-SCI, we quantified mCherry+rVRG fibers in sagittal spinal cord sections at various rostral-caudal distances relative to the lesion site. The schematic illustrates a sagittal section of the spinal cord, with the lighter grey area representing the lesion. Red lines symbolize mCherry-labeled rVRG axons, green triangles represent the PhMNs located caudal to the lesion, and dotted black boxes denote locations of the images in panels C-H (**A**). Quantification of numbers of mCherry-labeled fibers placed

into 100 μm rostral-caudal bins, with the rostral portion of the lesion serving as the zero point (**B**); * p value of ≤ 0.05. Representative images of spinal cord 1 mm rostral to the lesion site show similar numbers of mCherry labeled rVRG axons between the two groups (**C**-**D**); scale bar: 100 μm. In the intact spinal cord just rostral to the lesion, there were significantly more mCherry-labeled rVRG axons in AAV2-cRheb rats (**F**) compared to AAV2-GFP (**E**); scale bar: 100 μm. No mCherry+ axons were observed growing into the lesion with AAV2-GFP (E), while rVRG axons regenerated across the intact-lesion interface with cRheb expression (**F**); white dotted lines denote the rostral border of the lesion. At the lesion center (image approximately 300μm from the intact-lesion border), we observed regeneration of rVRG fibers with AAV2-cRheb (**H**), but none in AAV2-GFP animals (**G**); scale bars: 50 um. We analyzed multiple animals per group: n=4; we quantified 5 tissue sections per animal. Uninjured rats were injected AAV2-mCherry into the rVRG. 3 days prior to sacrifice, CTB was injected into the intraplueral space of the ipsliateral hemi-diaphragm, and rats were sacrificed at 7 weeks post-rVRG injection. We observed robust co-localization of mCherry-labeled rVRG fibers (**J**) with vGlut2-positive excitatory pre-synaptic terminals (**K**) and CTB-labeled PhMNs (**I**) in uninjured animals (overlay in **L**), showing synaptic connections between rVRG axons and all PhMNs; scale bar: 50 μM. Sagittal sections of the C4 spinal cord from laminectomy-only uninjured rats show CTB-labeled PhMNs (**M**) co-labeled with the trans-synaptic tracer WGA (**O**) residing in close spatial proximity to mCherry-labeled rVRG axons (**N**) (**P**: overlay); scale bar: 100 μm.

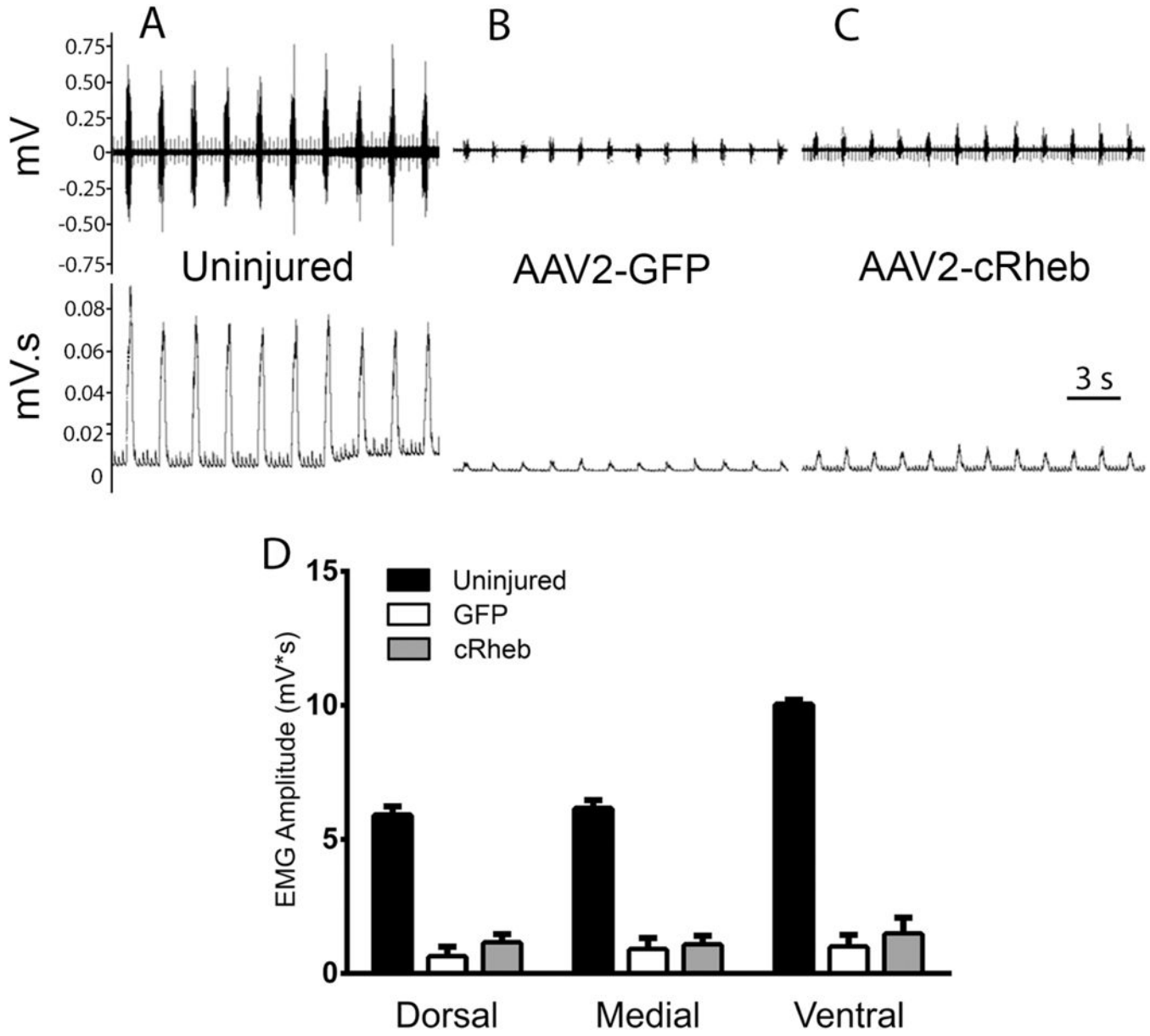

Figure 7. AAV2-cRheb transduction of rVRG neurons did not promote recovery of diaphragm function following C2 hemisection

Representative traces of electromyography (EMG) recordings from the medial portion of the hemi-diaphragm show a loss of approximately 80-90% amplitude in C2 hemisection animals injected with AAV2-GFP (**B**) or AAV2-cRheb (**C**) compared to uninjured controls (**A**). There were no differences between AAV2-cRheb and AAV2-GFP in burst amplitude at any of the three ipsilateral hemi-diaphragm sub-regions (**D**). Uninjured, AAV2-GFP, and AAV2-cRheb were quantified with n = 3, 4, and 7, respectively.